JOURNAL OF MATERIALS SCIENCE **35** (2000) 3365–3371

Texture development in Si_3N_4/BN fibrous monolithic ceramics

S. Y. LIENARD*, D. KOVAR
Texas Materials Institute and Department of Mechanical Engineering University of Texas at Austin, Austin, Texas 78712, USA
E-mail: dkovar@mail.utexas.edu

R. J. MOON, K. J. BOWMAN
Department of Materials Engineering, Purdue University, West Lafayette, IN 47907, USA

J. W. HALLORAN
Department of Materials Science and Engineering, University of Michigan, Ann Arbor, MI 48019, USA

Preferred orientation was measured in Si_3N_4/BN fibrous monolithic ceramics using x-ray diffraction. The materials were manufactured by co-extrusion of polymer binder/ceramic blends which were subsequently pyrolized and then hot-pressed to produced a fully dense ceramic composite. A very strong modified wire texture was present in the BN with the basal planes aligned parallel to the axis of extrusion due to shear-induced reorientation of the platelet-shaped BN particles during co-extrusion. Texture was also observed in the Si_3N_4 and was attributed to a combination of co-extrusion and hot-pressing. After hot pressing, the basal planes of the rod-shaped β-Si_3N_4 were observed to be preferentially aligned perpendicular to the extrusion direction. Measurements prior to hot-pressing revealed that a small amount ($\approx$5%) of β-Si_3N_4 was present in the α-Si_3N_4 starting powder. Although texturing of the predominant α-Si_3N_4 did not occur during co-extrusion, significant texturing of the β-Si_3N_4 was observed. During subsequent hot-pressing, the pre-existing textured β-Si_3N_4 particles appeared to act as seeds for transformation and preferred growth of rod-shaped β grains parallel to the axis of extrusion. © *2000 Kluwer Academic Publishers*

1. Introduction

Fibrous monolithic ceramics have potential as a low-cost alternative to fiber-reinforced ceramic matrix composites because they posses exceptional fracture resistance, yet they do not contain costly fibers [1]. Fibrous monolithic ceramics are manufactured by co-extrusion of relatively inexpensive polymer/ceramic powder blends [2]. After extrusion, the polymer is removed via pyrolysis and the fibrous monolithic ceramic is densified using traditional methods. A three-dimensional optical micrograph of the structure of a fibrous monolithic ceramic after densification by hot-pressing is shown in Fig. 1. The lighter cells consist of liquid-phase-sintered β-Si_3N_4 and the darker cell boundaries contain hexagonal BN.

Previous studies have shown that during fracture, cracks are inhibited from growing in a direction perpendicular the Si_3N_4 cells because crack deflection and delamination cracking occur within the weak BN cell boundaries. Extensive delamination cracking combined with frictional sliding between fractured cells have been shown to be responsible for the exceptional fracture resistance measured in these materials [3]. Fig. 2 is an SEM micrograph in the vicinity of a cell/cell boundary interface showing that the cell boundary consists of platelet-shaped BN grains that appear to be highly textured. TEM studies have confirmed that that the orientation of the basal planes of the BN lie parallel to the axis of the cell boundaries [4]. The combination of strong texture and easy basal cleavage appears to be responsible for the ease of delamination of the BN cell boundaries. In addition, there is evidence based on TEM micrographs that the Si_3N_4 is also textured [5]. Because texturing has been shown to significantly enhance the fracture resistance of Si_3N_4 [6, 7], it is likely that the properties of fibrous monolithic composites are also affected by texturing of the Si_3N_4. The purposes of the current study are to analyze the extent of texturing that is present in fibrous monolithic ceramics made from Si_3N_4 and BN, determine at which stage of processing texturing occurs, and determine the mechanisms for texture development.

* Exchange student from Science et Génie des Matériaux, Institut des Sciences et Techniques de Grenoble, Université Joseph Fourier de Grenoble, 38041 Grenoble, Cedex 9, France.

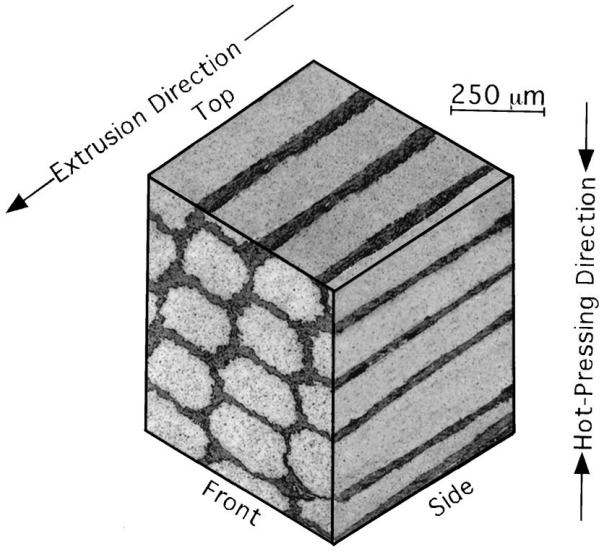

Figure 1 A three-dimensional optical micrograph of a fibrous monolithic ceramic after hot-pressing. The lighter colored cells are β-Si_3N_4 and the darker cell boundaries contain BN.

2. Experimental procedure

2.1. Specimen fabrication

As details of the procedures used to manufacture the materials have been presented elsewhere [1, 8, 9], we give only a brief summary here. In Fig. 3, a flow chart showing the processing steps used to manufacture the materials is shown. Si_3N_4 (M11, H.C. Starck Inc., Newton MA) and BN (HCP Grade, Advanced Ceramics Corp., Cleveland, OH) powders were milled separately in ethanol with a small amount of dispersant (Span 85, ICI Americas, Wilmington, DE). 6 wt% Y_2O_3 and 2 wt% Al_2O_3 were added to the Si_3N_4 powder as a sintering aid. After milling, the powders were dried and then individually compounded with a polymer binder and a plasticizer using a heated, high shear-rate mixer. The polymer/ceramic blends were then compression molded in heated steel dies to form a central core of Si_3N_4/polymer and two half-tubes of BN/polymer. The three pieces were assembled to form a feedrod with a diameter of 22 mm that contained approximately 83 vol% Si_3N_4/polymer and 17 vol% BN/polymer. The feedrod was co-extruded into a continuous, fine filament by forcing the feedrod through a heated spinerette with a diameter of 320 μm. The continuous filaments were chopped into lengths 75 mm long, stacked within a die, and compression molded to form a solid billet of aligned filaments. The polymer binder was removed by pyrolysis during slow heating to 700°C in a nitrogen atmosphere. The samples were subsequently hot-pressed at 1750°C for 2 hours under an applied pressure of 25 MPa with a nitrogen gas overpressure to densify the materials.

2.2. X-ray diffraction measurements

To determine the extent of texturing during the manufacturing process, representative samples were taken at each stage of fabrication and x-ray diffraction (XRD) was performed. In all cases, materials were cut into cube-shaped samples with dimensions approximately 3 mm by 3 mm by 3 mm. Green samples containing polymer were cut from a larger sample using a sharp, stainless steel scalpel and a fixturing device to ensure that all six sides of the cube were parallel and the angles between intersecting sides were 90°. Similar precautions were taken with the hot-pressed sample which was cut using a precision diamond saw.

X-ray diffraction measurements were made using standard Cu-K_α radiation operating at a scan speed of 0.3–1.5 °/min and at a step size of 0.05°. Because the beam size was much larger than the specimen size, the volume of material illuminated by the beam varied with the angle, θ, between the x-ray beam and the specimen. A correction was made by dividing the measured intensity by $\sin(\theta)$ to compensate for this effect. Measurements were taken on three perpendicular faces on each specimen corresponding to the top, side, and front faces of the cube (See Fig. 1 for a description of the geometry of the specimens.).

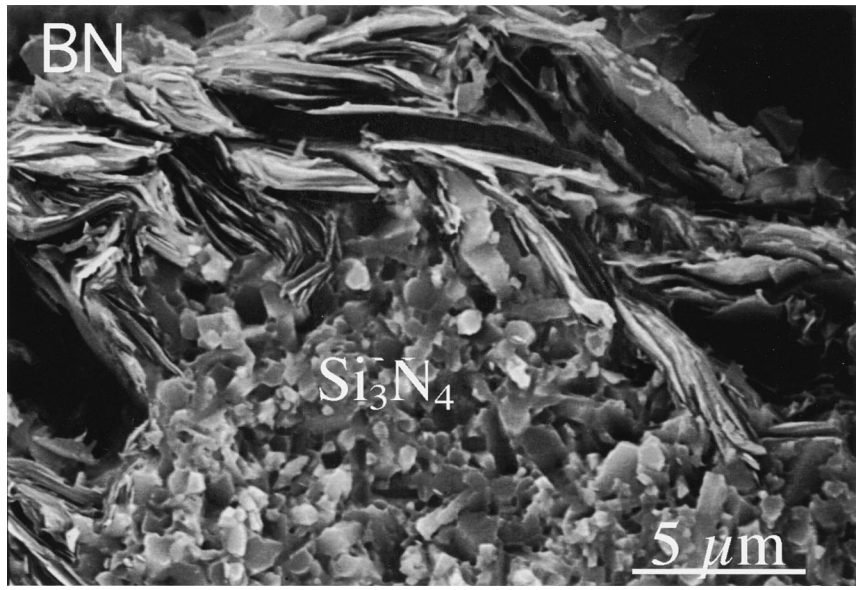

Figure 2 Fracture surface along the front face of a hot-pressed fibrous monolithic ceramic near the interface between a Si_3N_4 cell and a BN cell boundary. Note that almost all of the plate-shaped BN grains are aligned so that the basal planes are perpendicular to the plane of the page.

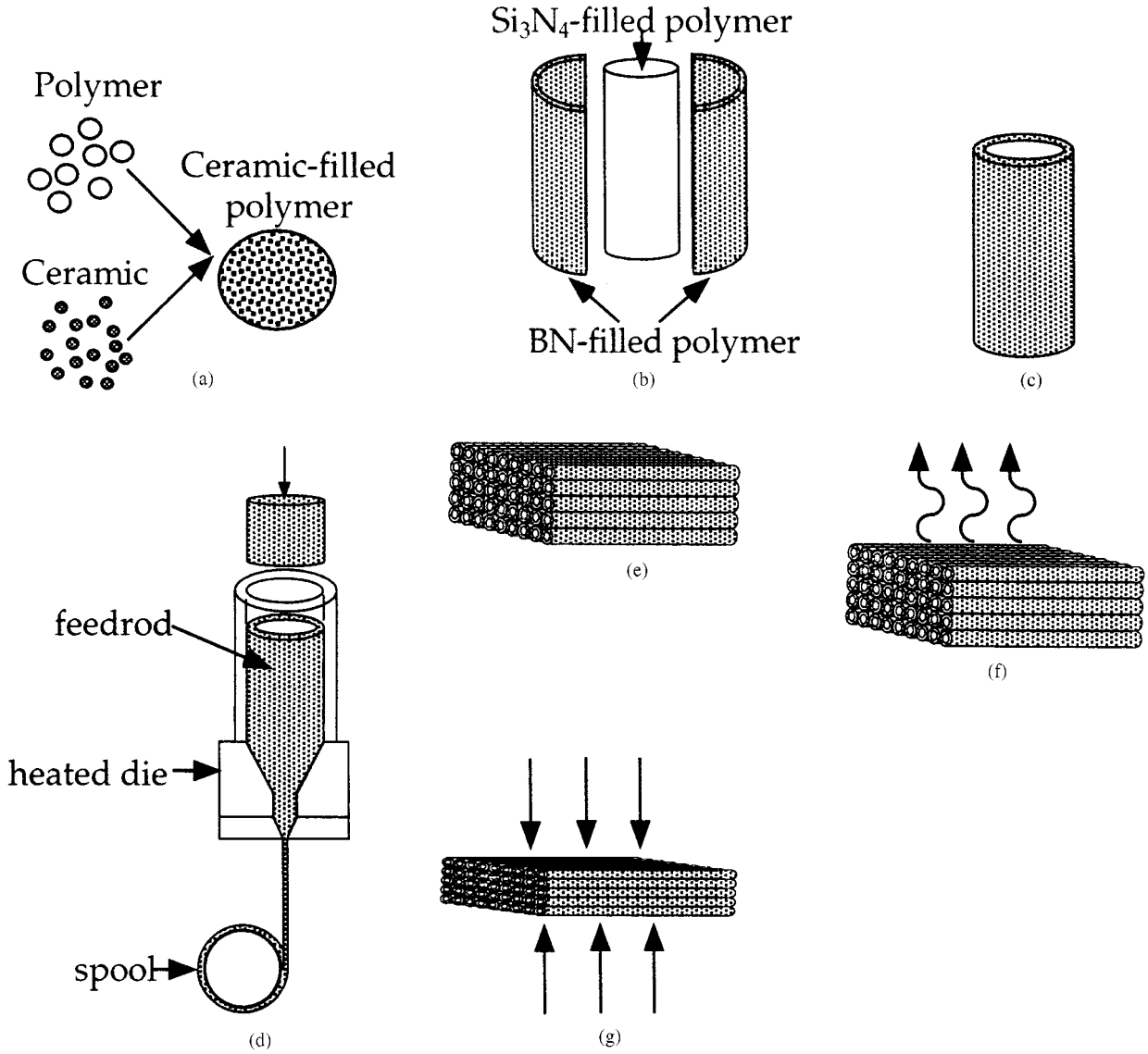

Figure 3 The sequence of manufacturing steps used to manufacture fibrous monolithic ceramics. a) The ceramic powders are blended with a polymer binder and plasticizer. b) The polymer/ceramic blends are compression molded separately into a central core and two half-tubes which are assembled to form a feedrod c). d) The feedrod is extruded into a fine filament by forcing it through a heated spinerette. e) The filament is chopped into lengths and compression molded to form a solid billet which is then pyrolized to remove the polymer f) and hot-pressed g).

There were several factors that limited our ability to quantify texture of BN in fibrous monolithic ceramics using a traditional method such as a pole figure analysis. Fibrous monolithic ceramics contain only about 18 vol% BN which reduced the overall intensities of the diffraction peaks from BN. In addition, BN has very few diffraction peaks with significant intensity and some of these overlap with the stronger Si_3N_4 peaks. Further, in most cases, BN was found to texture very strongly and only one significant diffraction peak was obtained. For these reasons, texture development in the BN was assessed only qualitatively. Texturing was measured for the silicon nitride by comparing the ratio peak intensities, after subtraction of the background, for the diffraction peaks from the (002) and (210) planes.

3. Results and discussion

3.1. Powder morphology

SEM and TEM micrographs in Fig. 4a and b show the shapes and sizes of the starting powder particles used to fabricate the fibrous monolithic specimens. According to the manufacturer, the Si_3N_4 powder consists of relatively equiaxed particles ranging in size from 0.1–1.5 μm with a specific surface area of 12–15 m^2/g. The powder is primarily α-Si_3N_4 but also contains a small fraction of β-Si_3N_4 (less than 10%). In contrast to the Si_3N_4 particles, the BN powder particles are distinctly anisometric with a plate-like morphology and a diameter of 0.5–3.0 μm and a thickness of 0.1–0.3 μm. TEM observation confirm that the large, flat face on each BN particle corresponds to the basal plane for each platelet [4].

3.2. Green feedrod

Fig. 5 shows X-ray diffraction patterns taken on the front and side faces of the green feedrod prior to extrusion showing diffraction peaks for BN and α-Si_3N_4. There is no distinction between the side and top faces because of the axial symmetry of the feedrod. The diffraction peaks for β-Si_3N_4 are not visible (confirming that the β content is quite low in the as-received

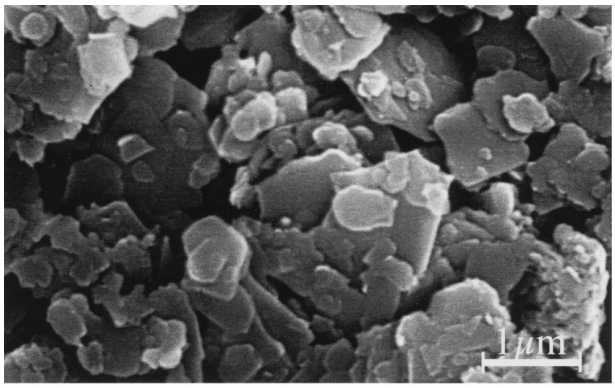

(a)

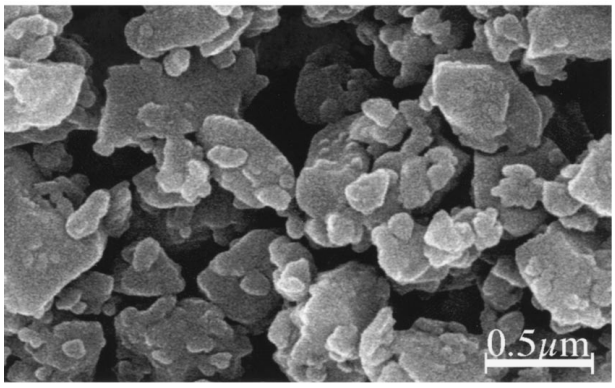

(b)

Figure 4 a) SEM micrograph of platelet-shaped BN powder particles. b) SEM micrograph of the as-received Si_3N_4 powder.

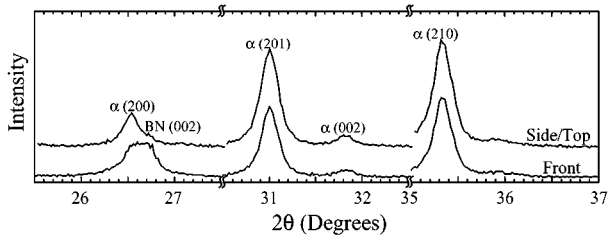

Figure 5 X-ray diffraction pattern of the top, side and, front faces of the green feedrod.

powders) and therefore are not analyzed in the feedrod. Instead, the ratio of intensities from the (002) and (210) peaks ($I_{\alpha(002)}/I_{\alpha}(210)$) for α-Si_3N_4 are compared. The extent of texturing is quantified by taking the ratio of measured peak intensities to theoretical peak intensities for the same diffraction peaks for untextured materials ($[I_{\alpha(002)}/I_{\alpha(210)}]_{\text{measured}}/[I_{\alpha(002)}/I_{\alpha(210)}]_{\text{theoretical}} = [I_{\alpha(002)}/I_{\alpha(210)}]/R_{\text{th}}$). Theoretical data for untextured materials is obtained from the JCPDS card for the relevant phases [10, 11]. From the data shown in Fig. 5, the ratio of the $(I_{\alpha(002)}/I_{\alpha(210)})/R_{\text{th}}$ is 0.94 while on the side face of the feedrod $(I_{\alpha(002)}/I_{\alpha(210)})/R_{\text{th}}$ is 1.2. The similarity between the measured values on different faces and the fact that they are both nearly one confirms that the α-Si_3N_4 is not significantly textured in the feedrod.

For the reasons discussed previously, there is some difficulty in quantifying the texture of the BN. However, meaningful information can be obtained from qualitative descriptions of the data. For example, on the front face of the feedrod, a significant BN-(002) peak is observed but this peak is completely absent on the side face. This indicates that the BN platelets within the feedrod are textured during the mixing or compression molding operations. The normal to the basal planes of the BN are preferentially aligned parallel to the axis of the feedrod. However, a significant amount of variability was observed in the texture of the BN in the feedrod depending on the location from which the specimen was cut. A small amount of food coloring added to the polymer/ceramic blends during shear mixing allowed flow lines to be readily observed in the feedrod. Based on these observations, it is clear that shear mixing introduces local regions of aligned platelets in the BN/polymer blends. Compression molding the feedrod from a large number of granules does not significantly alter the texture within the granules due to the limited flow that occurs during molding in a semi-closed die. As a result, the cladding of feedrod prior to extrusion consists of a patchwork of locally aligned regions of BN/polymer.

3.3. Extruded green fibrous monolithic ceramic

X-ray diffraction patterns for an aligned fibrous monolith after extrusion and compression molding are shown in Fig. 6 representing the top, side, and front faces of the cube. The relative peak intensities for BN are very different in the extruded sample compared to those observed in the feedrod prior to extrusion. Prior to extrusion, the BN-(002) peak is largest on the front face whereas after extrusion the BN-(002) peak is completely absent on the front face. Furthermore, the BN-(002) peak is now the largest peak on diffraction patterns taken from the top and side surfaces. This indicates that the character and the strength of the texture that is observed after compression molding of the feedrod is substantially altered during the extrusion process. In the extruded sample, the platelets are almost completely textured with the basal planes lying parallel to the extrusion direction.

A higher resolution diffraction pattern for the green extruded sample is shown in Fig. 7 so that texture in the α-Si_3N_4 can be more easily assessed. From this pattern, we see that the relative peak intensities for α-Si_3N_4 are similar to that observed in the green feedrod. For example, on the front face, $(I_{\alpha(002)}/I_{\alpha(210)})/R_{\text{th}}$ is 1.2 and $(I_{\alpha(002)}/I_{\alpha(210)})/R_{\text{th}}$ is 0.80 and 0.88 on the top and side faces, respectively. The similarity between measured intensity ratios on different faces and the fact that

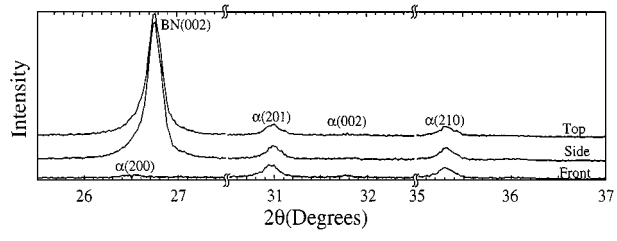

Figure 6 X-ray diffraction pattern of the top, side, and front faces of the extruded green filament after compression molding.

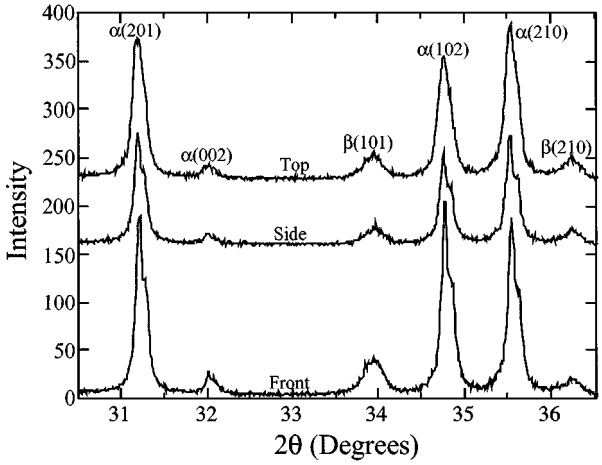

Figure 7 Higher resolution scan of the x-ray diffraction pattern shown in Fig. 6.

they are all nearly one indicates that the α-Si_3N_4 is not textured significantly during the extrusion process.

Quantification of the texture in the β-Si_3N_4 is complicated by the small fraction of β-Si_3N_4 present in the as-received powders and the inherently weak intensity of the β-(002) diffraction peak. However, because the α-Si_3N_4 is not significantly textured, the degree to which the β-Si_3N_4 is textured can be assessed by taking the ratio of $I_{\alpha(002)}/I_{\beta(210)}$. Since the theoretical ratio of $I_{\alpha(002)}/I_{\beta(210)}$ for an untextured material cannot be determined without knowing the exact fraction of α/β, this ratio only be used as a relative measure of texture. From the data shown in Fig. 7, this ratio is 2.3, 0.79, and 1.1 on the front, top and side surfaces. The large difference between the intensity on the front face compared to the top and side faces confirms that the β-Si_3N_4 is significantly textured during the extrusion process with the basal planes of the β-Si_3N_4 preferentially oriented perpendicular to the extrusion axis.

3.4. Hot-pressed fibrous monolithic ceramic

X-ray diffraction patterns for the top, side, and front faces of an aligned fibrous monolith are shown in Fig. 8 after removal of the polymer binder and after hot-pressing. No peaks are visible for α-Si_3N_4 because hot-pressing was performed above the $\alpha \rightarrow \beta$ transformation temperature. A large BN (002) peak is observed in the hot-pressed specimen on the top face. A somewhat smaller BN (002) peak is observed on the side face and the BN (002) peak is completely absent on the front face. This texture of the BN in the hot-pressed specimen is similar to that observed in the green extruded specimen, although the difference between the intensity of the BN (002) peak on the top and side surfaces is much greater in the hot-pressed specimen than in the green extruded specimen.

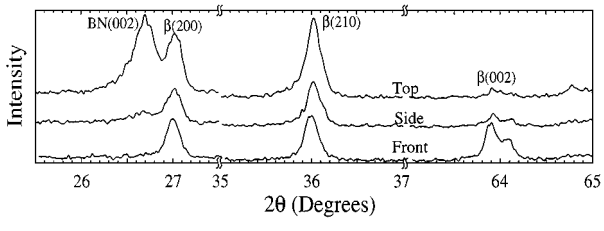

Figure 8 X-ray diffraction pattern of the top, side, and front faces of hot-pressed fibrous monolithic ceramic.

TABLE I A summary of the x-ray diffraction data for the BN in prior to extrusion, after extrusion, and after hot-pressing

	BN-$I_{(002)}$		
	Front	Top	Side
Prior to extrusion	Yes	No	No
After extrusion	No	Yes	Yes
After hot-pressing	No	Yes	Yes

TABLE II A summary of the x-ray diffraction data for the Si_3N_4 prior to extrusion, after extrusion, and after hot-pressing

	α-Si_3N_4 $(I_{(002)}/I_{(210)})/I_R$			β-Si_3N_4 $(I_{(002)}/I_{(210)})/I_R$		
	Front	Top	Side	Front	Top	Side
Prior to extrusion	0.94	1.2	1.2	—	—	—
After extrusion	1.2	0.80	0.88	—	—	—
After hot-pressing	—	—	—	3.1	0.52	0.76

TABLE III A summary of the x-ray diffraction data for the green co-extruded fibrous monolithic ceramic

	$I_{\alpha(002)}/I_{\beta(210)}$		
	Front	Top	Side
After extrusion	2.3	0.79	1.1

Comparison of the β-Si_3N_4 peaks for each of the three faces reveals that the β-Si_3N_4 is also textured significantly after hot-pressing. For example, β-$(I_{(002)}/I_{(210)})/R_{th}$ is 3.1 on the front face but 0.76 on the side surface and 0.52 on the top surface. Comparing $(I_{(002)}/I_{(210)})/R_{th}$ on the front surface to the side and top surfaces, it is clear that the texture in β-Si_3N_4 in the hot-pressed fibrous monolithic ceramic texture has the same general character as the β-Si_3N_4 observed in the green extruded specimen with basal planes preferentially aligned perpendicular to the extrusion axis. However, there is a slight difference between $(I_{(002)}/I_{(210)})/R_{th}$ on the top and side surfaces indicating a preferred texture in the plane of hot-pressing. A summary of the x-ray diffraction data is presented in Tables I–III.

4. Discussion

4.1. Texture development of BN

The texture observed in the BN is consistent with previous results in which texturing was observed during extrusion of whisker-loaded ceramic/polymer blends [12]. Anisometric particles were observed to align so that the long axis of the particles was parallel to the extrusion direction due to shear developed between the edges of the extrusion nozzle. A similar result is observed here except that the platelet-shaped morphology of the BN results in alignment of the flat faces of

the platelets (the basal plane) parallel to the extrusion direction. Similar alignment of platelets has also been observed during other forming processes that involve shearing of viscous fluids such as tapecasting [13, 14].

An examination of the diffraction patterns for the hot-pressed sample on the side and top faces reveals that the relative intensities for the (002) peak for BN are different on these two surfaces with significantly greater intensity on the top surface than on the side surface. This difference in intensity between the top and side surfaces was not observed in the green extruded specimen and therefore this texture must result from hot-pressing. The application of a force perpendicular to the top surface during hot-pressing results in a change in the shape of the cross section of the filaments. After extrusion, the green filaments have a nominally circular cross-section with the BN platelets aligned circumferentially around the filaments with their basal planes perpendicular to the extrusion direction. However, during hot-pressing the cross-section of the filaments is flattened so that the filaments are about twice as wide as they are tall. Although the platelets remain aligned circumferentially around the filaments, the shape of the filaments dictates that there is a greater probability that the basal planes of the BN platelets will lie parallel to the top surface than parallel to the side surface. This explains the development of the modified wire texture observed in the BN for hot-pressed fibrous monolithic ceramics.

4.2. Texture development in Si_3N_4

Texturing has been previously observed in monolithic ceramics such as tape-cast alumina [15, 16]. Nominally equiaxed alumina powders that were tapecast using a conventional doctor blade process resulted in a very slight texture in green alumina tapes. However, after firing, the tapes developed a strong texture with the basal plane aligned parallel to the casting direction. This texture was particularly strong near the surface but also existed within the bulk. It has been suggested that the texture is the result of preferred growth along low energy planes. However, the grains in these unseeded materials did not exhibit faceting and the grain shape remained nominally equiaxed. Further, subsequent experiments on liquid-phase sintered alumina [14] have shown that grains become *less* elongated after extensive annealing which would also seem to preclude a thermodynamic argument for achieving texture in these materials.

A second mechanism for achieving texture in ceramics with internal interfaces or surfaces is through constrained growth. Growing grains impinging on a surface or interface will cease to grow in that direction, biasing growth in a direction parallel to the surface or interface. This mechanism has been used to explain the observation that surfaces often tend to exhibit a greater degree of texture than the bulk [17]. In the materials used in this study, a large number of internal interfaces exist between the Si_3N_4 cells and the BN cell boundaries and thus constrained growth may occur within the Si_3N_4 cells. If this were the case, however, we would expect that there would be significant differences in the microstructure near the edge of a cell compared to near the center of the cell because β-Si_3N_4 has a strong tendency to facet which allows the orientation of the grains to be easily distinguished from the grain morphology. However, SEM observations did not indicate any obvious difference in the microstructure of the Si_3N_4 between the center of the cell and edge of the cell and therefore this mechanism also does not appear to explain the observed texture.

Stronger textures have been achieved in Al_2O_3 [13], SiC [18] and Si_3N_4 [6, 19] by intentionally introducing anisometric seeds crystals into the powder prior to forming. The seed crystals are aligned during the forming operation (extrusion, tape casting, or uniaxial pressing) and during sintering either act as seeds for epitaxial growth in a preferred direction or the seeds themselves grow consuming smaller surrounding matrix grains until they impinge on another growing seed. Seabaugh *et al.* [14] and Brandon *et al.* [20] suggested that if texturing occurs by the latter mechanism, the volume fraction of seed crystals and the size of the seed crystals relative to the matrix grains are the key variables that influence the resulting microstructure. They argued that crystallographically textured materials with aligned anisometric grain shapes are possible only when the size and volume fraction of the seed crystals is large compared to the matrix grains.

It has previously been reported that nominally equiaxed α-Si_3N_4 powder can be converted to $(\alpha+\beta)$-Si_3N_4 by heating at high temperatures and that the resulting β-Si_3N_4 particles are elongated along the $\langle 001 \rangle$ direction [17]. In the current study, no seed crystals were added to the powders but the as-received Si_3N_4 powder did contain a small fraction of β-Si_3N_4 which was aligned during co-extrusion. Although anisometric β particles were not readily discernible during an examination of the as-received powder in the TEM, this is not surprising given that the fraction of β-Si_3N_4 in these powders is relatively small. Nevertheless, the observed texture development during extrusion is consistent with the presence of anisometric β crystals elongated along the $\langle 001 \rangle$ direction. It appears that during hot-pressing, these preexisting β particles act as seeds for the $\alpha \rightarrow \beta$ transformation and for preferred growth in the extrusion direction.

Our results show that texturing of even a small fraction of particles during forming can result in significant texturing due to preferential grain growth during the sintering process. This can occur even if grain growth is normal; it is only necessary that 1) the seed particles be textured and 2) that they grow at the expense of the surrounding matrix grains. In the Si_3N_4 used in this study, this is achieved using a matrix of α-Si_3N_4 that is unstable at the sintering temperature and a small fraction of β-Si_3N_4 particles that texture during co-extrusion.

5. Conclusions

X-ray diffraction measurements on Si_3N_4/BN fibrous monolithic ceramics revealed that both the Si_3N_4 and the BN were textured during co-extrusion and subsequent hot-pressing. As expected, the plate-shaped BN

particles were aligned due to drag experienced in the shear field during co-extrusion. The character of the texture of the BN induced during co-extrusion was modified only slightly during subsequent hot-pressing. The commercially available Si_3N_4 powders used to manufacture these materials were found to contain a small fraction of β particles which aligned during co-extrusion. Upon hot-pressing, these textured β particles acted as sites for preferred growth which resulted in relatively strong texture in the direction of extrusion.

Acknowledgements

The authors would like to thank Mr. Dragan Popovic and Dr. Greg E. Hilmas of Advanced Ceramics Research (Tucson, AZ) for providing the green materials used in this study, Mr. Aaron Crumm (University of Michigan) for assistance in fabricating specimens, Dr. J. Steven Swinea (University of Texas at Austin) for assistance with the X- ray diffraction experiments and Prof. Lew Rabenberg (University of Texas at Austin) for his assistance with the TEM. Funding for this project was provided by DARPA and administered through ONR under contract #N0014-95-0302. SYL and DK would also like to acknowledge the support of the Bureau of Engineering Research at the University of Texas.

References

1. D. KOVAR, B. H. KING, R. W. TRICE and J. W. HALLORAN, *J. Amer. Ceram. Soc.* **80**(10) (1997) 2471.
2. D. POPOVIĆ, J. W. HALLORAN, G. E. HILMAS, G. A. BRADY, S. SOMMERS, A. BARDA and G. ZYWICKI, Patent no. 5,645,781 (1997).
3. D. KOVAR, M. D. THOULESS and J. W. HALLORAN, *J. Amer. Ceram. Soc.* **81**(4) (1998) 1004.
4. R. W. TRICE and J. W. HALLORAN, *ibid.*, **82** (1999) 2943.
5. R. W. TRICE, Ph.D. thesis. University of Michigan, 1998.
6. K. HIRAO, M. OHASHI, M. E. BRITO and S. KANZAKI, *J. Amer. Ceram. Soc.* **78**(6) (1995) 1687.
7. F. LEE, M. S. SANDIN and K. J. BOWMAN, *ibid.* **76**(7) (1993) 1793.
8. S. BASKARAN, S. D. NUNN, D. POPOVIC and J. W. HALLORAN, *ibid.* **76**(9) (1993) 2209.
9. G. HILMAS, A. BRADY, U. ABDALI, G. ZYWICKI and J. HALLORAN, *Mat. Sci. Eng. A* **A915** (1995) 263.
10. JCPDS no. 41-360 , Powder Diffraction File; edited by T.M. Kahmer *et al.* (International Centre for Diffraction Data, Newton Square, PA, 1997).
11. JCPDS no. 33-1160 , Powder Diffraction File; edited by T. M. Kahmer *et al.* (International Centre for Diffraction Data, Newton Square, PA, 1997).
12. Y. GOTO and A. TSUGE, *J. Amer. Ceram. Soc.* **76**(6) (1993) 1420.
13. T. CARISEY, I. LEVIN and D. G. BRANDON, *J. Eur. Ceram. Soc.* **15**(4) (1995) 283.
14. M. M. SEABAUGH, I. H. KERSCHT and G. L. MESSING, *J. Amer. Ceram. Soc.* **80**(5) (1997) 1181.
15. F. V. DIMARCELLO, P. L. KEY and J. C. WILLIAMS, *ibid.* **55**(10) (1972) 509.
16. Y. NAKADA and T. L. SCHOCK, *ibid.* **58**(9/10) (1975) 409.
17. Y. GOTO, A. TSUGE and K. KOMEYA, *J. Eur. Ceram. Soc.* **6**(4) (1990) 269.
18. M. D. SACKS, G. W. SCHEIFFELE and G. A. STAAB, *J. Amer. Ceram. Soc.* **79**(6) (1996) 1611.
19. K. HIRAO, K. WATARI, M. E. BRITO, M. TORIYAMA and S. KANZAKI, *ibid.* **79**(9) (1996) 2485.
20. D. BRANDON, D. CHEN and H. CHAN, *Mat. Sci. Eng. A* **A195**(1/2) (1995) 189.

Received 13 April
and accepted 16 December 1999